ELSEVIER

Materials Science and Engineering A247 (1998) 187–194

MATERIALS SCIENCE & ENGINEERING A

Texture evolution in NiAl

K.E. Harris [a], F. Ebrahimi [b], H. Garmestani [a,*]

[a] *Department of Mechanical Engineering, FAMU-FSU College of Engineering, Tallahassee, FL 32306, USA*
[b] *Department of Materials Science and Engineering, University of Florida, Gainesville, FL 32611, USA*

Received 5 December 1996; received in revised form 20 October 1997

Abstract

We have investigated texture evolution in stoichiometric NiAl and Ni-49at.%Al–1at.%Ti using orientation imaging microscopy (OIM) and X-ray diffraction. Grain size and orientation were studied after extrusion and after heat treatment, leading to the following model of texture evolution. During extrusion, dynamic recrystallization occurs with a continuing cycle of deformation to produce a $\langle 110\rangle$ fiber texture, nucleation of nearly randomly-oriented grains, and preferential growth of $\langle 111\rangle$ grains. Upon cooling from the extrusion temperature, nucleation continues until the temperature drops below the recrystallization temperature. A $\langle 110\rangle$ fiber texture observed after extrusion suggests the specimen did not fully recrystallize during cooling and the deformation texture is retained. A $\langle 111\rangle$ fiber texture indicates a fully recrystallized microstructure in which significant grain growth has occurred. It has been found that titanium addition increases the recrystallization temperature of NiAl and retards grain growth resulting in the retention of the $\langle 110\rangle$ fiber texture. © 1998 Elsevier Science S.A. All rights reserved.

Keywords: X-ray diffraction; Recrystallization; Extrusion; Fiber

1. Introduction

NiAl has been investigated extensively over the past few decades because its high thermal conductivity, low density, and excellent oxidation resistance makes it a promising high temperature structural material, but its application has been hampered by its poor low temperature ductility and high temperature strength (See [1,2] for recent reviews). Slip in NiAl occurs primarily on $\langle 100\rangle\{011\}$ and $\langle 100\rangle\{010\}$ systems, providing only three independent slip systems [3], and the resulting incompatibility between grains during straining causes intergranular cracking of polycrystalline NiAl [1,2,4]. In both metallic and ceramic materials, low energy boundaries such as low-angle boundaries and low-Σ boundaries have been shown to be resistant to intergranular fracture, while high angle random boundaries are preferential sites for crack nucleation and propagation [5]. Since the grain boundary character distribution is related to the distribution of grain orientations [6–8], understanding the evolution of crystallographic texture in NiAl may lead to the ability to modify the cracking behavior.

Several investigations of the texture of extruded NiAl have been carried out recently [9–15]. High temperature extrusions or annealing have been shown to result in a $\langle 111\rangle$ fiber texture aligned with the extrusion direction [9–15]. This texture has been attributed to recrystallization [9–13,15] or grain growth [14]. After extrusion at lower temperatures a $\langle 110\rangle$ fiber texture has been observed [9,14] and this texture is most often referred to as a deformation texture [9,11]. A deformed microstructure was described in connection with a $\langle 110\rangle$ texture of a specimen hydrostatically extruded at 573 K [12], but in other reports, microstructures of specimens with $\langle 110\rangle$ texture have been described as recrystallized with equiaxed grains [9,13–15]. In an alternate explanation, Bieler et al. [14] have suggested that the $\langle 110\rangle$ texture may be a nucleation texture, rather than a deformation texture, which, after extrusion at high temperatures or annealing, is consumed by the preferential growth of grains with $\langle 111\rangle$ orientations.

The purpose of this study has been to understand the origins of the $\langle 110\rangle$ and $\langle 111\rangle$ textures in stoichiometric NiAl. Addition of titanium has been shown to improve the high temperature strength of NiAl signifi-

* Corresponding author. Tel: +1 904 6445993; fax: +1 904 6441227.

0921-5093/98/$19.00 © 1998 Elsevier Science S.A. All rights reserved.
PII S0921-5093(97)00740-5

cantly [4,16], therefore an alloy consisting of Ni-49at.%Al–1at.%Ti has also been investigated. These alloys were studied in as-extruded (AE) and heat-treated (HT) conditions. We have used the relatively new capabilities of orientation imaging microscopy (OIM) [19], as well as X-ray diffraction, to gain insight into the mechanisms of texture evolution in NiAl. OIM employs the computer acquisition and indexing of electron back scatter patterns (EBSPs) from an array of points to obtain orientations of a large number of grains in a specimen. Once the orientation and position of the grains are known, direct correlations between texture and other microstructural characteristics such as grain size and grain boundary character can be made through the creation of orientation maps. The computer automation in OIM provides for a more thorough examination of the microstructure than possible with manual transmission electron microscopy (TEM) or scanning electron microscopy (SEM) single grain diffraction pattern analysis.

2. Materials and methods

The two different compositions examined were NiAl (Ni-50at.%Al) and Ni-49at.%Al–at.%Ti (hereafter referred to as NiAl + Ti). The original material was vacuum induction melted, cast in copper molds and then extruded in steel cans at a 12:1 ratio, with a final extrusion diameter of 13 mm. The NiAl alloy was extruded at 1150 K and the NiAl + Ti alloy at 1175 K. Heat treatment at 1273 K for 1 h was carried out in flowing argon.

Transverse and longitudinal sections of the AE and HT specimens were prepared for microstructural analysis. (The end portions of the extrusion were discarded before sectioning) The samples were mechanically polished and electropolished in a solution of 5% perchloric acid in methanol. Kroll's reagent (2 ml HF + 4 ml HNO_3 + 94 ml H_2O) was used for etching the grain structure for SEM imaging.

A Philips MRD X-ray diffractometer was used to collect {220}, {111} and {200} pole figures from the transverse sections. A modified WIMV algorithm [17] implemented in the software package, preferred orientation package from Los Alamos (popLA) [18] was used to calculate the sample orientation distributions from which inverse pole figures were produced.

In OIM, electron back scattered patterns (EBSPs) formed in a SEM are collected from points on the sample surface distributed over a regular grid and automatically indexed. From this data, a map can be constructed displaying changes in crystal orientation over the specimen surface. The orientation of each point in the microstructure is known and hence the location, line length and character of all grain boundaries. For discussions of EBSPs and OIM, see [19,20].

To form an EBSP, the specimen was tilted 70° to the horizontal, a stationary electron probe was placed on a single-crystal region of the specimen, and the diffraction pattern was imaged on a phosphor screen placed close to it. For the experiments described below, the distance between the screen and the specimen was 2.2 cm. The phosphor screen was viewed through an optical port using a high gain television camera which was interfaced to a computer. The camera control unit was used to average eight video images of the pattern and enhance the pattern by dividing the averaged pattern image by a background image obtained by scanning over a large number of grains.

Some explanation of the definition of a 'grain' in OIM is necessary to understand the implications of the OIM maps described below. In OIM, a grain is a set of connected points with similar orientations. The user defines a tolerance angle, the maximum misorientation two neighboring points in the same grain may have. The grain-defining algorithm then looks at the microstructure point by point. For each point in the microstructure, the neighboring points are checked and the misorientation is compared to the tolerance angle. If the misorientation between two neighboring points is greater than the tolerance angle, the two points are identified as belonging to two different grains. If it is less than the tolerance angle, they are identified as belonging to the same grain. The neighbors of these points are then checked, and so on until the set of connected points is bounded by points which exceed the tolerance angle. For example, OIM maps produced with a 10° tolerance angle were used to investigate the NiAl and NiAl + Ti specimens. For these images, the point-to-point variation in orientation must be $< 10°$, but the cumulative variation in orientation across an entire grain may be larger.

3. Results

SEM micrographs of the transverse and longitudinal sections of the AE specimens are shown in Fig. 1. In both the transverse and longitudinal sections, the AE microstructures have equiaxed grains. Significant grain growth occurred during annealing in both alloys. The mean grain sizes for NiAl (HT) and NiAl + Ti (HT) are 84 and 27 μm, respectively. The grain sizes in the AE specimens show more variation with mean sizes of 12 and 9 μm for NiAl (AE) and NiAl + Ti (AE), respectively. As seen in Fig. 1(a) and (b), the etched surfaces of some of the grains appear rough. Apparently the etchant attacks defects in NiAl and produces pit-like features on the surface. These etch pits may correspond to dislocations or point defect clusters.

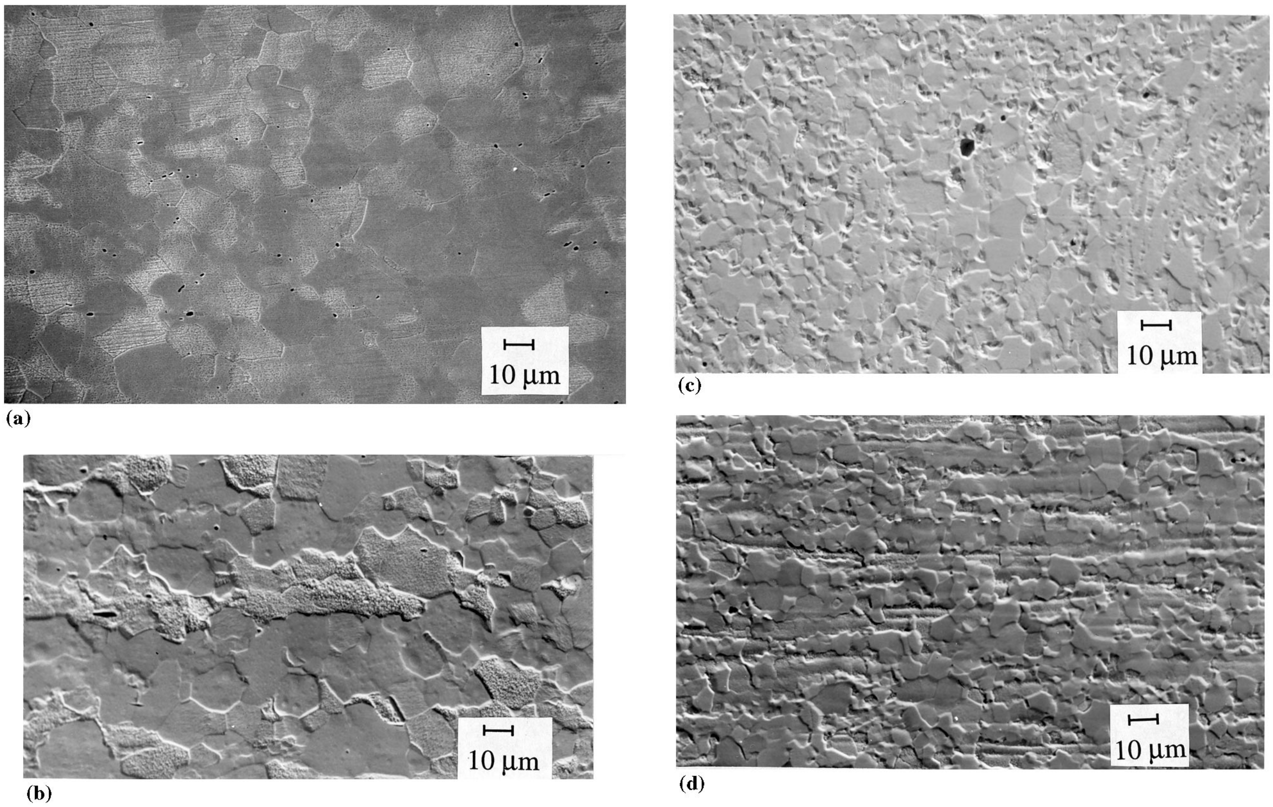

Fig. 1. SEM micrographs of NiAl, as extruded, transverse section (a), longitudinal section (b), and NiAl + Ti, as-extruded, transverse section (c) and longitudinal section (d).

Electron microprobe analysis of an unetched specimen has revealed that the composition of the NiAl + Ti is inhomogeneous, with titanium content varying from 0.5 to 2.0%. These concentrations are below the solubility limit for titanium in NiAl [21], and no precipitates are expected to form. As can be seen in Fig. 1(d), the NiAl + Ti alloy microstructure shows deeply etched grooves which are parallel to the extrusion axis. It has been found that the regions with highest titanium concentration correlate with the regions that etch deeply in the AE microstructure. It is suggested that during solidification, titanium is pushed into the interdentritic regions, which subsequently elongate during extrusion.

The X-ray diffraction inverse pole figures showing the distribution of crystal plane normals that are parallel to the extrusion direction are presented in Fig. 2. The AE specimens both have a ⟨110⟩ fiber texture as indicated by the high intensity around the location of the ⟨110⟩ poles, but the NiAl + Ti (AE) has a much stronger ⟨110⟩ preferred orientation (ten times random) than the NiAl (AE) (4.3 times random). Upon annealing, the intensity of the ⟨110⟩ component decreases, and the intensity of the ⟨111⟩ component increases. Overall, the texture is more random after annealing.

OIM maps were collected from transverse sections of each specimen, and one representative map from each section will be discussed. Unless indicated otherwise, the OIM maps were drawn using a 10° grain tolerance angle. Large angle grain boundaries (LABGs), defined as having misorientation $>10°$, are identified with thick black lines, and small angle grain boundaries (SAGBs) defined as having misorientation between 2

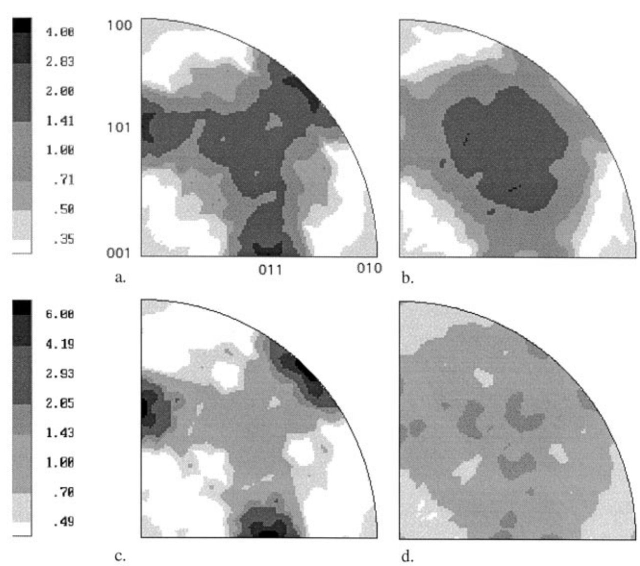

Fig. 2. Equal area projection inverse pole figures for (a) NiAl (AE); (b) NiAl (HT); (c) NiAl + Ti (AE) and (d) NiAl + Ti (HT).

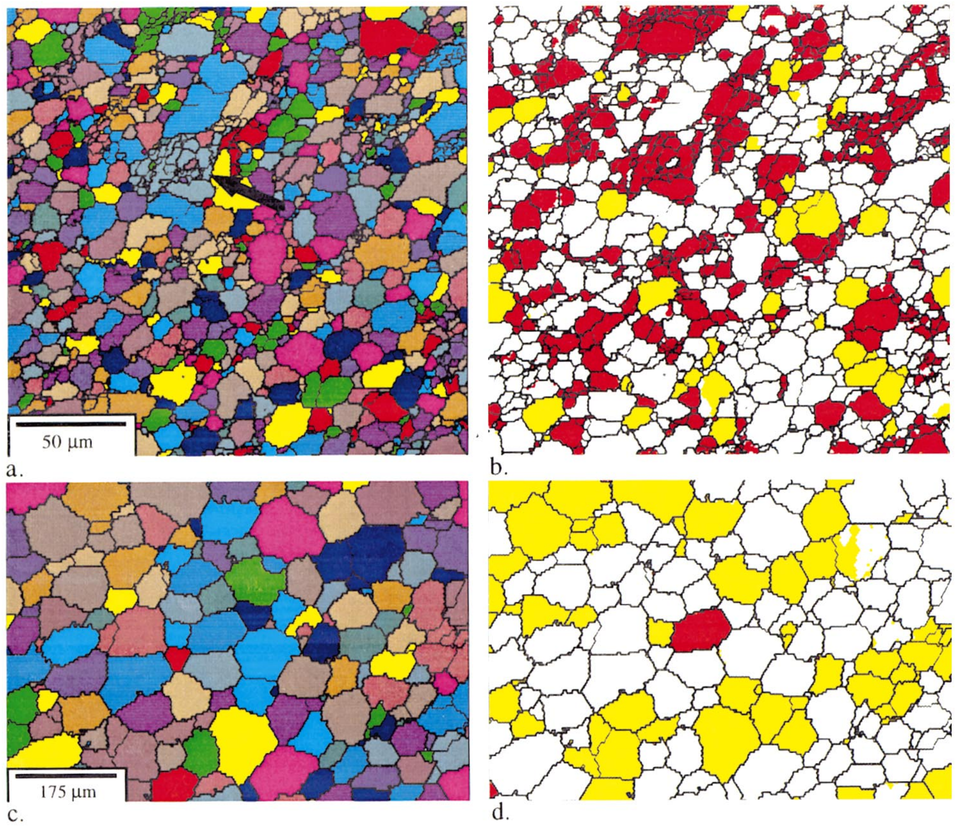

Fig. 3. (a) OIM map of NiAl (AE), 10° tolerance angle, 1 μm step size; (b) OIM map with ⟨111⟩ grains and ⟨110⟩ grains colored yellow and red, respectively; (c) OIM map of NiAl (HT), 10° tolerance angle, 5 μm step size; (d) OIM map with ⟨111⟩ grains and ⟨110⟩ grains colored yellow and red, respectively. Thin and thick grain boundaries identify misorientations between 2 and 10° and 10 and 180°, respectively.

and 10°, are identified with thin black lines. The colors used to shade the grains in Fig. 3(a) and (c), Fig. 5(a), (c), (d) and (e) are applied to aid the eye in identifying different grains; the color does not indicate any property of the grain. For Fig. 3(b) and (d), Fig. 5(b) and (f), grains with normals within 10° of ⟨111⟩ are colored yellow and those with normals within 10° of ⟨110⟩ are colored red.

OIM maps for NiAl (AE) collected using a step size of 1 μm are shown in Fig. 3(a) and (b). These images show the microstructure is primarily composed of equiaxed grains defined by LAGBs, however grains with irregular shapes and SAGBs in their interiors are also observed. One such grain is indicated by the arrow in Fig. 3(a). Approximately 60% of these grains have orientations within 10° of ⟨110⟩ as indicated by red shading in Fig. 3(b). This can also be seen by looking at the discrete inverse pole figures for individual grains, shown in Fig. 4. Orientations of regions having SAGBs are shown in Fig. 4(a) and those having no SAGBs in Fig. 4(b). Here we see clearly the strong ⟨110⟩ texture of the regions with SAGBs. Fig. 3(b) also reveals that grains with ⟨111⟩ orientations tend to be larger than other grains. Mean grain sizes for ⟨110⟩ and ⟨111⟩ grains are compared with the grain size for all grains in Table 1. The fraction of the image occupied by ⟨110⟩ and ⟨111⟩ grains is also indicated in Table 1. The area fraction of the microstructure with ⟨110⟩ orientation is greater than that with ⟨111⟩ orientation which agrees qualitatively with the relative intensities of the ⟨110⟩ and ⟨111⟩ texture components (4.3 and 1.7 times random, respectively) in the X-ray inverse pole figure shown in Fig. 2(a).

OIM maps of NiAl (HT), collected using a step size of 5 μm are shown in Fig. 3(c) and (d). These maps reveal a fully recrystallized microstructure with

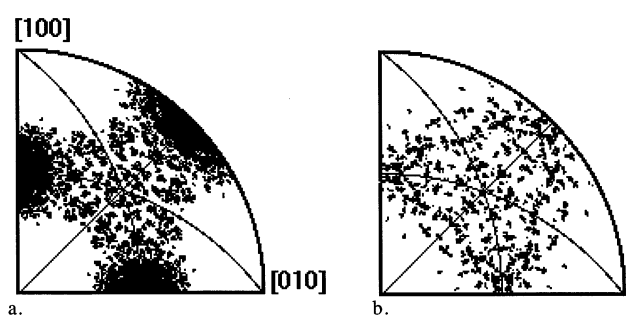

Fig. 4. Equal angle projection discrete inverse pole figures for NiAl (AE) for grains with SAGBs in their interiors (a) and grains with no SAGBs (b).

Table 1
Mean grain area, standard error in the mean grain area, grain dimension (length of a side of a hexagon with equivalent area) and area fractions for each specimen and for grains with ⟨111⟩ and ⟨110⟩ in the extrusion direction

Specimen	Grain area (μm^2)	Standard error (μm^2)	Grain dimension (μm)	Area fraction
NiAl (AE)	56	3	9	
⟨111⟩	81	3	11	0.098
⟨110⟩	53	15	9	0.269
NiAl (HT)	2857	238	66	
⟨111⟩	3558	404	74	0.377
⟨110⟩	1174	472	42	0.017
NiAl+Ti (AE)	8.9	2.7	3.7	
⟨111⟩	5.6	1.1	2.9	0.017
⟨110⟩	15.6	10.0	4.9	0.572
NiAl+Ti (HT)	418	34	25	
⟨111⟩	250	52	20	0.031
⟨110⟩	588	63	30	0.166

equiaxed grains and a decrease in the fraction of ⟨110⟩-oriented grains in agreement with the decrease in intensity of the ⟨110⟩ component of texture measured by X-ray. The mean size of the ⟨111⟩ grains is larger than the mean size of the ⟨110⟩ grains.

The OIM maps of NiAl + Ti (AE) shown in Fig. 5(a) and (b)were collected using a step size of 0.5 μm. For NiAl + Ti (AE), the irregularly-shaped, ⟨110⟩-oriented regions with SAGBs are much more prominent than in NiAl (AE) and the grain size of the equiaxed grains is much smaller. The discrete inverse pole figures for regions with and without SAGBs are shown in Fig. 6(a) and (b), respectively. As seen for NiAl (AE), the inverse pole figure for the regions with SAGBs shows the strong ⟨110⟩ preferred orientation.

In order to see the large ⟨110⟩-oriented regions better, a second scan of NiAl + Ti (AE) was carried out using a step size of 1 μm. Maps created from this scan are shown in Fig. 5(c) and (d). In Fig. 5(c), the tolerance angle is set to 10°. The grain sizes of the three largest ⟨110⟩-oriented regions seen here are 5119, 2236 and 1533 μm^2. The OIM map correlates better with the SEM image shown in Fig. 1 if plotted using a 5° tolerance angle, shown in Fig. 5(d). In this map, the population of small equiaxed grains dominates the microstructure in agreement with the SEM images. This correlation indicates that the etchant used to define the microstructure for SEM imaging attacked both small and large angle boundaries. The differences in the grain morphology of NiAl and NiAl + Ti suggests that titanium is important to the microstructural evolution. This is considered in more detail in the discussion section below.

OIM maps of NiAl + Ti (HT), collected using a step size of 2 μm, are shown in Fig. 5(e) and (f). Fig. 5(e) shows a fully recrystallized microstructure similar to that observed in NiAl (HT), but Fig. 5(f) shows a smaller fraction of ⟨111⟩-oriented grains and a larger fraction of ⟨110⟩-oriented grains than NiAl (HT). The majority of the grains have neither ⟨111⟩ nor ⟨110⟩ orientations in agreement with the X-ray inverse pole figures which indicate a randomization of the texture compared to the strong ⟨110⟩ preferred orientation observed in the AE case.

4. Discussion

The ⟨110⟩ fiber textures evident in the inverse pole figures obtained by X-ray diffraction of the AE specimens are in good agreement with results reported for other low temperature extrusions of NiAl [9,14]. While the SEM images in Fig. 1 show a microstructure with equiaxed grains, OIM can discriminate between large and small angle boundaries, thus providing a different picture of the microstructure. In the OIM maps for NiAl (AE) and NiAl + Ti (AE), we see both irregularly-shaped grains with SAGBs and small equiaxed grains. This two-component microstructure indicates that dynamic recrystallization has occurred during extrusion, as suggested by Dymek et al. [11]. During dynamic recrystallization the microstructure is in a continuous cycle of nucleation, growth and deformation with different volume fractions of grains at different stages of the cycle [22]. The nucleation, growth and deformation stages may each produce a different preferred orientation. While cooling from the extrusion temperature, the material can continue the nucleation process until the temperature decreases below the recrystallization temperature. Any deformed regions present at this point can continue to recover until the combination of internal stresses and temperature drops too low for dislocation motion.

In the OIM maps of NiAl + Ti (AE) shown in Fig. 5(a), (b) and (c) we see the most drastic contrast between the large irregularly-shaped regions with strong ⟨110⟩ fiber texture and regions with very small equiaxed grains and a more random orientation. Dur-

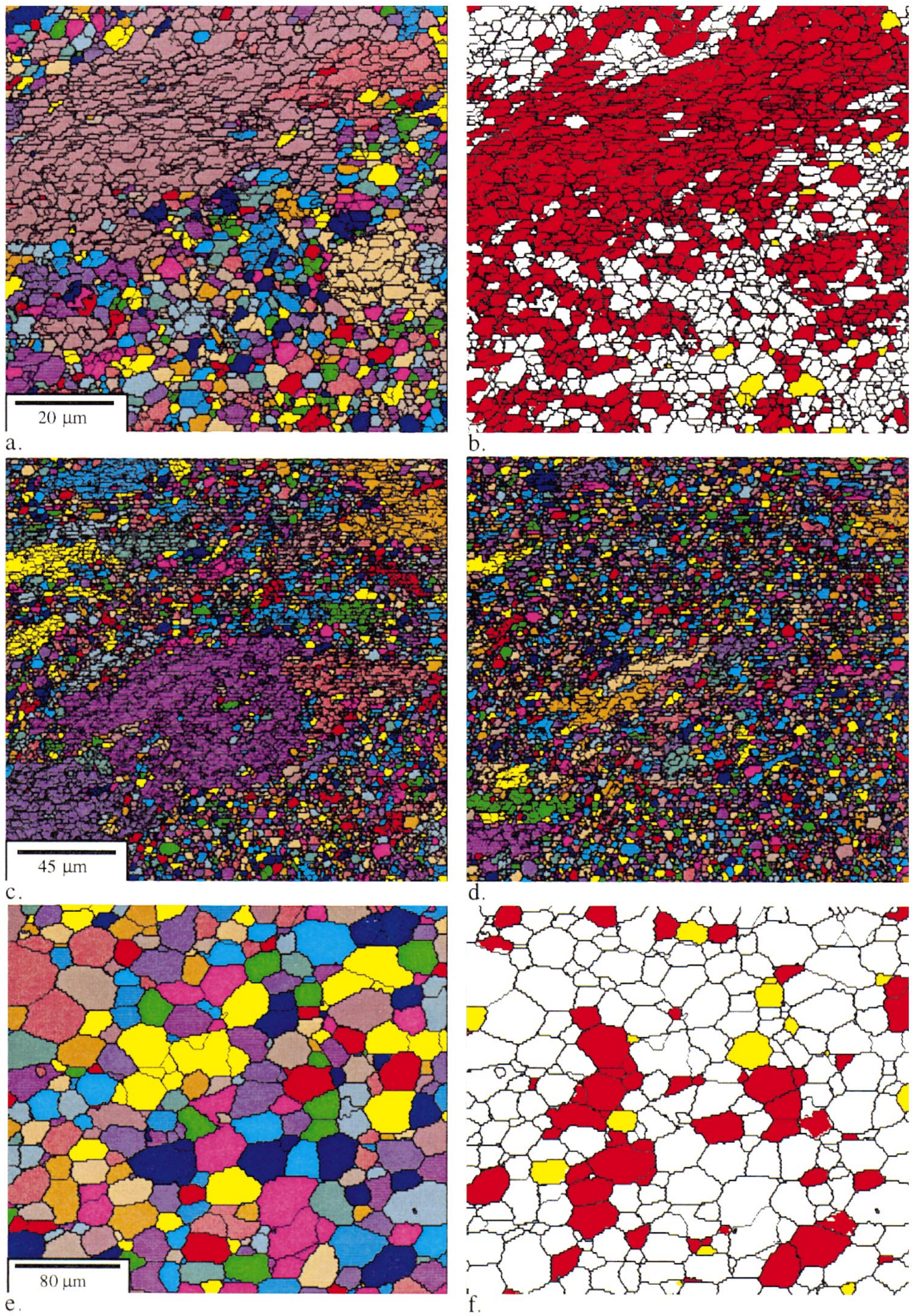

Fig. 5. (a) OIM map of NiAl + Ti (AE), 10° tolerance angle, 0.5 μm step size; (b) OIM map with ⟨111⟩ grains and ⟨110⟩ grains colored yellow and red, respectively. (c) OIM map of NiAl + Ti (AE), 10° tolerance angle, 1 μm step size. (d) OIM map with 5° tolerance angle; (e) OIM map of NiAl + Ti (HT), 10° tolerance angle, 2 μm step size; (f) OIM map with ⟨111⟩ grains and ⟨110⟩ grains colored yellow and red, respectively. Thin and thick grain boundaries identify misorientations between 2 and 10° and 10 and 180°, respectively.

ing extensive deformation, a very narrow texture distribution can develop as grains rotate such that neighboring grains have nearly the same orientation, separated only by small misorientations. Such a deformed region would appear as the large ⟨110⟩-oriented regions observed in NiAl + Ti. Alternatively, the large ⟨110⟩-oriented regions may be deformed grains from the as-cast microstructure which have not undergone recrystallization. In either case we see the ⟨110⟩ texture does in fact result from deformation as suggested by [9,11]. The size of the irregularly-shaped ⟨110⟩ grains in NiAl (AE) is approximately the same as the mean grain size and is much smaller than the grain size of the cast microstructure, suggesting that the

⟨110⟩ grains in this specimen were formed by dynamic recrystallization.

The ⟨110⟩-oriented regions are most prominent in NiAl + Ti (AE), indicating that titanium in solid solution increases the recrystallization temperature as expected based on the increase in tensile strength of Ti-containing NiAl [4,14]. During cooling the temperature will drop below the recrystallization temperature quickly, and most of the remaining deformed microstructure will only be able to undergo recovery, thus 'freezing in' the deformation texture. In NiAl (AE), the recrystallization temperature is lower, so recrystallization can continue longer during cooling. As a result we see primarily recrystallized equiaxed grains with only a few of the irregularly-shaped ⟨110⟩-oriented regions.

The OIM inverse pole figures in Fig. 4(b) and Fig. 6(b) show that the recrystallized grains do not have a strong preferred orientation. In the OIM maps of the AE specimens, we see ⟨111⟩-oriented grains as a part of the population of recrystallized grains in the AE specimens, and in NiAl (AE) these ⟨111⟩-oriented grains are larger than the mean grain size. Their larger size suggests that they may have special high mobility boundaries which give them an advantage for growth over the other grains. The ⟨111⟩ grains grow preferentially during annealing as seen in the OIM results from NiAl (HT), where the fraction of the microstructure occupied by grains with ⟨111⟩ orientation is higher and the fraction with ⟨110⟩ orientation is lower than in NiAl (AE) in correspondence with the texture transition observed in the X-ray diffraction results. A ⟨111⟩ fiber texture is commonly observed in NiAl extruded at higher temperatures ($T > 1100°C$) and is retained or strengthened by annealing, so it has often been attributed to recrystallization [9–13]. While a strong ⟨111⟩ fiber texture similar to those reported for high temperature extrusions [9–15] never develops in our specimens, our OIM observations indicate that the ⟨111⟩ fiber texture may be more specifically defined as a growth texture rather than a recrystallization texture; it is only by preferential growth of ⟨111⟩-oriented grains that we see an increase in the ⟨111⟩ fiber texture component. The observed decrease in ⟨110⟩ texture component suggests that the grains in the recovered regions do not grow during annealing, but are consumed by growth of the recrystallized grains. Further investigation into the grain boundary character in these specimens may provide the information required to understand the contribution of grain growth to the evolution of texture in NiAl.

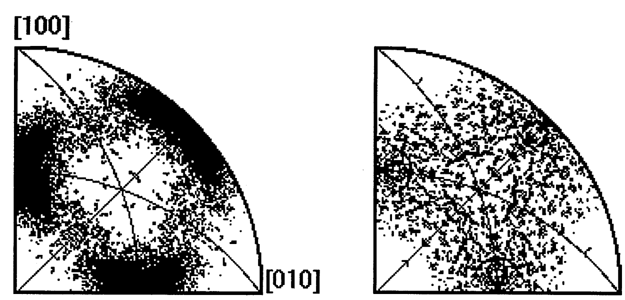

Fig. 6. Equal angle projection discrete inverse pole figures for NiAl + Ti (AE) for grains with SAGBs in their interiors (a) and grains with no SAGBs (b).

We do not see much of an increase in the fraction of grains with ⟨111⟩ orientation in NiAl + Ti during annealing. The presence of titanium is seen to increase the recrystallization temperature as mentioned above. The smaller grain size of the recrystallized grains in NiAl + Ti (AE) and the limited grain growth in the HT specimen suggests that the addition of titanium retards the diffusivity of atoms in NiAl and may possibly modify the grain boundary structure. A more detailed investigation of the microstructure evolution is required to fully understand how the texture develops in this specimen, but it is anticipated that annealing at higher temperatures may produce accelerated growth and a corresponding increase in the < 111 > texture component.

5. Conclusion

Our investigation of extruded NiAl using OIM suggests the following model for microstructural evolution during and after extrusion. During extrusion dynamic recrystallization occurs with a continuing cycle of deformation to produce a ⟨110⟩ fiber texture, nucleation of new nearly randomly-oriented grains, and preferential growth of ⟨111⟩ grains. Upon cooling from the extrusion temperature, nucleation continues until the temperature drops below the recrystallization temperature. If deformation remains at this point, only recovery can take place and the deformation texture is frozen in. A ⟨110⟩ texture observed after extrusion suggests the specimen did not fully recrystallize during cooling and the deformation texture is retained, while a ⟨111⟩ texture indicates a fully recrystallized microstructure in which significant grain growth has occurred.

Acknowledgements

K. Harris and H. Garmestani gratefully acknowledge the financial support of the Center for Materials Research and Technology, and F. Ebrahimi acknowledges the financial support of the Air Force Office of Scientific Research under URI Grant No. F49620-93-1-030. The authors thank Dr J.D. Whittenberger of NASA Lewis Research Center for providing the alloys used in this study, and K. Harris thanks Dr M.L. Weaver for metallography assistance and many helpful discussions during the course of this research.

References

[1] R.D. Noebe, R.R. Bowman, M.V. Nathal, Int. Mater. Rev. 38 (1993) 193.
[2] D.B. Miracle, Acta Metall. Mater. 41 (1993) 649.
[3] J.D. Cotton, M.J. Kaufman, R.D. Noebe, Scr. Metall. Mater. 25 (1991) 2395.
[4] F. Ebrahimi, T.G. Hoyle, Acta Mater. 45 (1997) 4193.
[5] T. Watanabe, Mater. Sci. Forum 46 (1989) 23.
[6] A. Garbacz, M.W. Grabski, Scr. Metall. 23 (1989) 1369.
[7] V. Randle, B. Ralph, D. Dingley, Acta Metall. 36 (1988) 267.
[8] A. Morawiec, J.A. Szpunar, D.C. Hinz, Acta Metall. Mater. 41 (1993) 2825.
[9] T.R. Bieler, R.D. Noebe, M. Hebsur, R. Saminathan, in: J.J. Jonas, T.R. Bieler, K.J. Bowman (Eds.), Advances in Hot Deformation Textures and Microstructures, TMS, Warrendale, PA, 1994, p. 519.
[10] P.S. Khadkikar, G.M. Michal, K. Vedula, Metall. Trans. A 21A (1990) 279.
[11] S. Dymek, S.J. Hwang, M. Dollar, J.S. Kallend, P. Nash, Scr. Metall. Mater. 27 (1992) 161.
[12] R.W. Margevicius, J.J. Lewandowski, Scr. Metall. Mater. 29 (1993) 1651.
[13] R.W. Margevicius, J.D. Cotton, Acta Metall. Mater. 43 (1995) 645.
[14] T.R. Bieler, R.D. Noebe, J.D. Whittenberger, M.J. Luton, in: D.B. Miracle, D.L. Anton, J.A. Graves (Eds.), Intermetallic Matrix Composites II, Mater. Res. Soc. Symp. Proc. 273 (1992), Pittsburgh, PA, p. 165.
[15] S.-J. Hwang, Ph.D. Dissertation, Illinois Institute of Technology, IL, 1992.
[16] W.S. Walston, R.D. Field, J.R. Dobbs, D.F. Lahrman, R. Darolia, in: R. Darolia, J.J. Lewandowski, C.T. Liu, P.L. Martin, D.B. Miracle, M.V. Nathal (Eds.), Structural Intermetallics, TMS, Warrendale, PA, 1993, p. 523.
[17] S. Mathies, G.W. Vinel, Phys. Status Solidif. B 112 (1982) 111.
[18] J.S. Kallend, U.F. Kocks, A.D. Rollett, H.-R. Wenk, Mater. Sci. Eng. A132 (1991) 1.
[19] D.J. Dingley, V. Randle, J. Mater. Sci. 27 (1992) 4545.
[20] S.L. Wright, B.L. Adams, K. Kunze, Metall. Trans. 24A (1993) 819.
[21] R. Yang, N. Saunders, J.A. Leake, R.W. Cahn, Acta Metall. Mater. 40 (1992) 1553.
[22] T. Sakai, J.J. Jonas, Acta Metall. 32 (1984) 189.